

# Symmetries and conserved quantities of boundary time crystals in generalized spin models

Giulia Piccitto,<sup>1,\*</sup> Matteo Wauters,<sup>2,\*</sup> Franco Nori,<sup>3,4</sup> and Nathan Shammah<sup>5,3,6</sup>

<sup>1</sup>*SISSA, Via Bonomea 265, I-34135 Trieste, Italy*

<sup>2</sup>*Niels Bohr International Academy and Center for Quantum Devices, Copenhagen University, Universitetsparken 5, 2100 Copenhagen, Denmark*

<sup>3</sup>*Theoretical Quantum Physics Laboratory, RIKEN Cluster for Pioneering Research, Wako-shi, Saitama 351-0198, Japan*

<sup>4</sup>*Physics Department, University of Michigan, Ann Arbor, Michigan, 48109-1040, USA*

<sup>5</sup>*Unitary Fund*

<sup>6</sup>*Quantum Technology Lab, Dipartimento di Fisica, Università degli Studi di Milano, 20133 Milano, Italy*

(Dated: May 30, 2022)

We investigate how symmetries and conserved quantities relate to the occurrence of the boundary time crystal (BTC) phase in a generalized spin model with Lindblad dissipation. BTCs are a non-equilibrium phase of matter in which the system, coupled to an external environment, breaks the continuous time translational invariance. We perform a detailed mean-field study aided by a finite-size analysis of the quantum model of a  $p,q$ -spin-interaction system, a generalized  $p$ -spin-interaction system, which can be implemented in fully-connected spin- $\frac{1}{2}$  ensembles. We find the following conditions for the observation of the BTC phase: First, the BTC appears when the discrete symmetry held by the Hamiltonian,  $\mathbb{Z}_2$  in the considered models, is explicitly broken by the Lindblad jump operators. Second, the system must be coupled uniformly to the same bath in order to preserve the total angular momentum during the time evolution. If these conditions are not satisfied, any oscillatory behavior appears only as a transient in the dynamics and a time-independent stationary state is eventually reached. Our results suggest that these two elements may be general requirements for the observation of a stable BTC phase relating symmetries and conserved quantities in arbitrary spin models.

## I. INTRODUCTION

Non-equilibrium quantum many-body systems are one of the modern paradigms of research in quantum physics. Indeed, they represent one of the key elements to control and manipulate mesoscopic quantum systems and, therefore, they lie at the root of the growing field of quantum technologies [1–4]. Moreover they display a wide range of non-trivial dynamics [5–17] and host a plethora of interesting phenomena with no analogue in equilibrium states [18–27]. Of particular interest are many-body driven-dissipative quantum systems [28, 29], where dissipation and decoherence can radically change the critical properties of phase transitions [30, 31] and induce an extremely rich steady-state phase diagram.

In recent years, considerable attention has been drawn by the so-called time crystals [32–34], a phase of matter characterized by a spontaneous breaking (in the thermodynamic limit) of the time-translational symmetry, that in short-ranged systems is impossible to realize at equilibrium [35, 36]. In their most common form, they are a sub-harmonic response to a periodic driving, thus breaking a *discrete* time-translational symmetry [37–39].

More interestingly, a time crystal might appear also when there is no explicit time dependence in the Hamil-

tonian but the system is subjected to incoherent processes [40–42]. In this particular case, known as *Boundary Time Crystals* (BTC), an open system self-organizes in a time-periodic pattern, with a frequency that depends only on the model’s relevant energy scales and on the strength of the coupling with the environment. From an experimental point of view, this phenomenon is very appealing because it *relies* on the presence of dissipation, while, usually, time-order is destroyed by the inevitable decoherence effects [43] present in experimental setups.

BTCs have been first introduced in the context of fully connected spin models, where permutational invariance [44–46] allows the exact numerics up to rather large systems [47–55] and makes the mean-field description particularly reliable [44, 56–61]. In contrast to discrete time crystals, however, little is still understood about the conditions needed for the emergence of the BTC phase.

An interesting topic is that of the relation between BTCs and symmetries. The role of the symmetries in the open-system dynamics has been already under discussion [62, 63], especially in the case of open systems with decoherence-free subspaces [62, 64–69]. Although BTCs share some phenomenology with them, they have different physical roots. The BTC phase, indeed, is well defined only in the thermodynamic limit, where periodic oscillations with the same frequency are observed for any initial condition. On the other hand, if the dynamics has decoherence-free subspaces, a non-stationary behavior may emerge after an initial relaxation at any system size. In particular, symmetry-preserving dissipation con-

---

\* These two authors contributed equally to this work  
gpiccitto@sissa.it  
wauters@nbi.ku.dk

curs to split the non-decaying part of the Hilbert space into disjoint sectors, leading to permanent oscillations with a frequency directly inherited from the Hamiltonian [70].

In Ref. [40], it has been shown that both a free spin in a static magnetic field and the fully connected Ising model exhibit a transition from a normal phase to a time-ordered one, driven by the system-environment coupling strength, when all spins coupled to the same bath through a collective [71] operator. However, an apparent contradiction emerged in Ref. [72], where no evidence of time-ordering was found in the closely related  $p$ -spin model, where  $p$  refers to the order of the highest interaction in the Hamiltonian,  $p > 2$ .

In this work we solve this seeming contrast and clarify the mechanism behind the onset of persistent oscillations in the expectation values of physical observables. To this purpose, we consider a generalized  $p$ -spin Hamiltonian, coupled to the environment via Lindblad operators – the model can be implemented in a fully-connected spin- $\frac{1}{2}$  ensemble with collective dissipation, analogously to Refs. [40, 72]. The dissipative dynamics is studied by combining a mean-field approach and an exact finite-size analysis, where we solve directly the Lindblad master equation [73, 74] for the density matrix  $\hat{\rho}$ .

We find that BTCs survive when two elements are simultaneously present. First, the Hamiltonian part of the model possesses a discrete symmetry,  $\mathbb{Z}_2$  for the collective spin- $\frac{1}{2}$  system, which must be explicitly broken by the operators coupling the system with the environment. The model used in Refs. [72], contrarily to Ref. [40], does not satisfy this symmetry requirement, hence explaining the absence of BTCs. Second, the system must have a strong symmetry, namely an observable that commutes both with the Hamiltonian and the Lindblad operators. This requirement is fulfilled by including in the open-system dynamics only collective incoherent processes, as was guessed in Refs. [41, 52], meaning that all sites need to be coupled uniformly to global baths. Physically, this is related to the presence of a conserved quantity, which in the considered spin models is the total angular momentum.

In the absence of either one of the two conditions, we find that the system always relaxes towards a stationary state, time-translational invariance is recovered in the long-time limit and all information on the initial condition is lost. When both are satisfied, instead, the boundary time crystal phase is present; at the mean-field level, it is identified by the presence of closed periodic trajectories in the semiclassical phase space, while in finite sizes it is revealed by oscillations with a damping rate diverging in the thermodynamic limit. Supported by numerical evidence in a study including dissipation to ever increasing bath sizes – ranging from local to collective –, we argue that these elements may be necessary conditions for the existence of BTCs in general spin systems, beyond homogeneous fully-connected spin models.

Interestingly, also the finite-size density matrix  $\hat{\rho}_0$  of

the stationary state can identify the BTC phase: when time-order is present in the thermodynamic limit,  $\hat{\rho}_0$  cannot be approximated by a well-defined mean-field ansatz, but rather it is the average over all the states on the time-crystal trajectory [75].

The article is organized as follows: In Sec. II we introduce the model we investigate and its mean-field description. In Sec. III we review some of the main results known in the literature within the more general framework we present in this paper. Our main results are presented in Sec. IV, where we focus on the symmetry requirements to the BTC phase, and in Sec. V, where we show the effects of non-collective Lindblad operators. In Sec. VI we discuss possible experimental realizations of boundary time-crystals. Finally, we summarize our findings in Sec. VII.

## II. THEORETICAL FRAMEWORK

We consider a generalization of the well know  $p$ -interacting spin model [76–79] described by the Hamiltonian ( $\hbar = 1$ )

$$\hat{H} = -N \left( \omega_z \hat{J}_z^p + \omega_x \hat{J}_x^q \right), \quad (1)$$

with  $p, q \in \mathbb{N}$  and the spin algebra is given by  $[\hat{J}_x, \hat{J}_y] = i2\hat{J}_z/N$ ,  $[\hat{J}_+, \hat{J}_-] = 2\hat{J}_z/N$ , where, without loss of generality, we consider these as collective spins from a system of  $N$  all-to-all interacting spin- $\frac{1}{2}$ .  $\hat{J}_\alpha = \sum_i \hat{\sigma}_i^\alpha/N$  are the (collective) magnetization operators and  $\hat{\sigma}_i^\alpha$  are the Pauli matrices acting on the  $i$ -th site. The dynamics we consider is given by the Lindblad master equation [73, 80]

$$\begin{aligned} \frac{d}{dt} \hat{\rho} = & -i[\hat{H}, \hat{\rho}] + N\Gamma^\uparrow \left( \hat{J}^+ \hat{\rho} \hat{J}^- - \frac{1}{2} \{ \hat{J}^- \hat{J}^+, \hat{\rho} \} \right) \\ & + N\Gamma^\downarrow \left( \hat{J}^- \hat{\rho} \hat{J}^+ - \frac{1}{2} \{ \hat{J}^+ \hat{J}^-, \hat{\rho} \} \right), \end{aligned} \quad (2)$$

where  $\hat{J}^\pm = \hat{J}_x \pm i\hat{J}_y$  describe two collective incoherent processes with associated rates  $\Gamma^{\uparrow(\downarrow)}$ . Note that Eq. (2) in general couples the spin ensemble to two separate baths, as the  $\Gamma^{\uparrow(\downarrow)}$  rates can be independently chosen. This includes the case of a single bath at detailed balance, in which  $\Gamma^\uparrow = \Gamma_0(1 + n_T)$ , and  $\Gamma^\downarrow = \Gamma_0 n_T$  due to the favored spin alignment in the upward direction of Eq. (1), with  $n_T$  the thermal occupation number, which goes to zero at  $T = 0$ , and  $\Gamma_0$  a coefficient fixed for the considered model. Depending on the largest between  $\Gamma^\downarrow$  and  $\Gamma^\uparrow$ , the Lindblad operators favor spin alignment along the upward ( $\hat{J}^+$ ) or the downward ( $\hat{J}^-$ )  $z$  direction, explicitly breaking the  $\mathbb{Z}_2$  symmetry the Hamiltonian displays for  $p$  even.

Notice that Eq. (2) preserves the total angular momentum  $\hat{J}^2$ , which is a *strong symmetry* [65, 66] of the set of generalized spin models considered,  $[\hat{H}, \hat{J}^2] = [\hat{J}_-, \hat{J}^2] =$

$[\hat{J}_+, \hat{J}^2] = 0$ . Moreover, besides for the treatment of local baths performed in Sec. V, hereafter we can generalize the models beyond their derivation in terms of collections of spin- $\frac{1}{2}$ , and consider them genuine  $(N + 1)$ -spins, further opening up quantum simulation experimental possibilities, as detailed in Sec. VI.

The mean-field equations of motion for the expectation values of the magnetization operators  $X, Y, Z = \langle \hat{J}_x \rangle, \langle \hat{J}_y \rangle, \langle \hat{J}_z \rangle$  are obtained with a Gutzwiller approximation,  $\langle \hat{J}_\alpha \hat{J}_\beta \rangle = \langle \hat{J}_\alpha \rangle \langle \hat{J}_\beta \rangle$ , where  $\alpha, \beta = x, y, z$  and  $\langle \cdot \rangle = \text{Tr}[\hat{\rho} \cdot]$  is the expectation value on the state  $\hat{\rho}$ . With this approximation, the equations for the macroscopic variables are

$$\begin{cases} \dot{X} = 2p\omega_z Z^{p-1} Y - 2\delta\Gamma Z X, \\ \dot{Y} = 2XZ (q\omega_x X^{q-2} - p\omega_z Z^{p-2}) - 2\delta\Gamma Z Y, \\ \dot{Z} = -2q\omega_x Y X^{q-1} + 2\delta\Gamma(1 - Z^2), \end{cases} \quad (3)$$

with  $\delta\Gamma = \Gamma^\uparrow - \Gamma^\downarrow$  (the full derivation can be found in App. A).

We introduce in notation  $\dot{\mathbf{R}} = (\dot{X}, \dot{Y}, \dot{Z})$  and study the solutions of this system for  $\dot{\mathbf{R}} = 0$ , i.e.  $\mathbf{R} = (X_{\text{st}}, Y_{\text{st}}, Z_{\text{st}})$  are the stationary states of the dynamics. In what follows, we refer to a *ferromagnetic* stationary state if  $|Z_{\text{st}}| > 0$  and to a *paramagnetic* one if  $Z_{\text{st}} = 0$ . The real part of the eigenvalues of the associated Jacobian, i.e. the real part of the Lyapunov exponents, provides a classification of the stationary states: if all the eigenvalues have positive (negative) real part, the trajectories are attracted toward (repelled from) the relative state. More interestingly, if the real part is zero and the Lyapunov exponents are purely imaginary [81] we are in presence of a marginal fixed point generating periodic orbits, and the stationary state is associated with a BTC trajectory [82].

When studying a finite size system, a fundamental role is played by the structure of the Liouvillian superoperator [80, 83–87]  $\mathcal{L}$ , defined through Eq. (2) as  $\dot{\rho} = \mathcal{L}[\rho]$ . For a finite system size  $N$ , in general, the spectrum of  $\mathcal{L}$  is gapped and the dynamic relaxes towards a stationary state  $\hat{\rho}_0$ , defined as the right eigenvector of  $\mathcal{L}$  with eigenvalue  $\lambda_0 = 0$ . The other eigenvectors, instead, are associated with eigenvalues  $\lambda_{i \neq 0}$  with  $\text{Re}[\lambda_{i \neq 0}] < 0$  and give information on the transient dynamics. For instance, the real part of the first nonzero eigenvalue  $|\text{Re}[\lambda_1]|$ , the Liouvillian gap, describes the relaxation rate.

The BTC phase, instead, is characterized by the presence of at least one complex eigenvalue (and its complex conjugate) whose real part vanishes in the thermodynamic limit, while the imaginary part saturates to a constant value [75, 88]. In this case, the real and the imaginary parts of the eigenvalues are associated with the damping of the oscillations in finite systems and to their frequency, respectively.

### III. BOUNDARY TIME CRYSTALS IN $p, q$ -INTERACTING SPIN MODELS: AN OVERVIEW

To exemplify our findings, we start with reviewing the results known in the literature: the Ising Hamiltonian with  $z$ -interactions ( $p = 2$  and  $q = 1$ ), and the Ising Hamiltonian with  $x$ -interactions ( $p = 1$  and  $q = 2$ ), both in the presence of dissipation, which have been studied in Refs. [40] and [72], respectively. Here we want to summarize the main features that will be essential for what comes next.

#### A. Free spins ( $p = 1, q = 1$ )

Before proceeding let us briefly comment on the case of free spins in a magnetic field lying in the  $x$ - $z$ -plane. The Hamiltonian reads ( $p = 1, q = 1$  in Eq. (1))

$$\hat{H}^{\text{free}} = -N \left( \omega_z \hat{J}_z + \omega_x \hat{J}_x \right). \quad (4)$$

Without loss of generality, we take  $\omega_x, \omega_z \geq 0$  throughout the whole paper.

The limit  $\omega_x = 0$  is trivial: we have two possible ferromagnetic stationary solutions  $\mathbf{R} = (0, 0, \pm 1)$ , obtained by solving  $\dot{\mathbf{R}} = 0$ ; one of them is stable and the other is unstable, depending on the sign of  $\delta\Gamma$ . When  $\omega_z = 0$ , as discussed in [40], the system has two different phases divided by the critical value of the dissipation  $\delta\Gamma_c = \omega_x$ : for  $\delta\Gamma < \delta\Gamma_c$  the system is in a BTCs phase, while for  $\delta\Gamma > \delta\Gamma_c$  the system again has two stationary states  $\mathbf{R} = (0, 0, \pm 1)$ . As soon as  $\omega_z > 0$ , the system falls inevitably in the ferromagnetic phase, where the time crystal order is destroyed and there are only trivial solutions with magnetization  $Z = \omega_z / \sqrt{\omega_x^2 + \omega_z^2 - \delta\Gamma^2}$ .

#### B. $z$ -interactions ( $p = 2, q = 1$ )

Let us now move to the fully connected Ising chain in transverse field, with interactions along the  $z$  direction described by the Hamiltonian ( $p = 2, q = 1$  in Eq. (1))

$$\hat{H}^{(z)} = -N \left( \omega_z \hat{J}_z^2 + \omega_x \hat{J}_x \right). \quad (5)$$

Without loss of generality, let us assume  $\omega_x > 0$ . The mean-field equations in Eq. (3) have four fixed points, two ferromagnetic solutions, and two paramagnetic ones.

The ferromagnetic solutions are given by

$$\mathbf{F}_\pm = \left( \frac{2\omega_x \omega_z}{4\omega_z^2 + \delta\Gamma^2}, \frac{\delta\Gamma \omega_x}{4\omega_z^2 + \delta\Gamma^2}, \pm \sqrt{1 - \frac{\omega_x^2}{4\omega_z^2 + \delta\Gamma^2}} \right), \quad (6)$$

one of which is stable and the other unstable, in fact the system is attracted toward the positive or negative magnetization state depending on the sign of  $\delta\Gamma$ . From

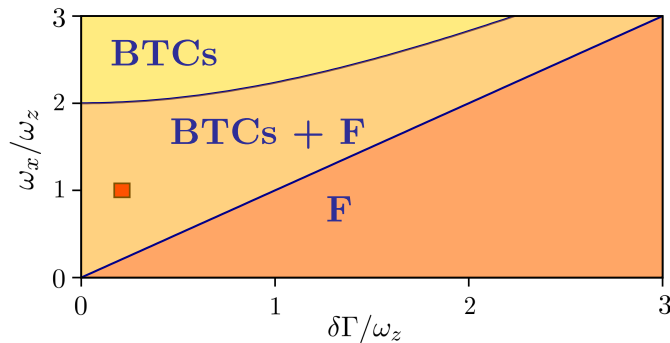


FIG. 1. Phase diagram of the system in Eq. (5), with  $z$ -interactions and  $x$ -driving in the Hamiltonian and collective dissipation greater than collective incoherent pumping,  $\delta\Gamma > 0$ . We plot the class of solutions as a function of the driving  $\omega_x$  and the dissipation rate  $\delta\Gamma$  both in units of  $\omega_z$ . F means that we have ferromagnetic solutions only, BTCs that we have marginal solutions only, F + BTCs means that both phases coexist. The red square marks the parameters used in Fig. 2.

the constraint  $X^2 + Y^2 + Z^2 = 1$  we deduce the existence condition for these solutions  $\omega_x < \omega_{x_c} = \sqrt{4\omega_z^2 + \delta\Gamma^2}$ .

The two paramagnetic solutions are

$$\mathbf{P}_{\pm} = \left( \pm \sqrt{1 - \frac{\delta\Gamma^2}{\omega_x^2}}, \frac{\delta\Gamma}{\omega_x}, 0 \right), \quad (7)$$

which exist only when the dissipation rate is smaller than the transverse field  $\delta\Gamma \leq \omega_x$ . Among the two, the most interesting is the negative one, since it is the marginal point that acts as the generator of the periodic orbits characterizing the BTC phase.

Having gathered this information, we can draw the phase diagram in Fig. 1, in which we show the phases of the system as a function of  $\omega_x$  and  $\delta\Gamma$ , both in unit of  $\omega_z$ : the system has a ferromagnetic phase (F) for  $\delta\Gamma > \omega_x$ , a BTCs phase for  $\omega_x > \sqrt{4\omega_z^2 + \delta\Gamma^2}$  and a region where they coexist. Note that values of  $\delta\Gamma > \omega_z$  are attainable in driven systems whose interaction-picture Hamiltonian takes the form of Eq. (3), even if dissipation mechanisms are perturbative effects [89]. Here the dynamics depends on the initial condition: the closer the parameters  $\omega_x$  and  $\delta\Gamma$  are to the purely ferromagnetic phase, the larger is the basin of attraction for the corresponding fixed point. In the opposite situation, close to the boundary with the BTC phase, most of the initial conditions lead to periodic trajectories while a small number of them relaxes towards the ferromagnetic point.

A more intuitive way to visualize this information is by looking at the phase portrait obtained by studying the dynamics in polar coordinates, which correspond to the parametrization

$$\mathbf{R} = (\sin \theta \cos \varphi, \sin \theta \sin \varphi, \cos \theta), \quad (8)$$

see appendix B for more details on the derivation.

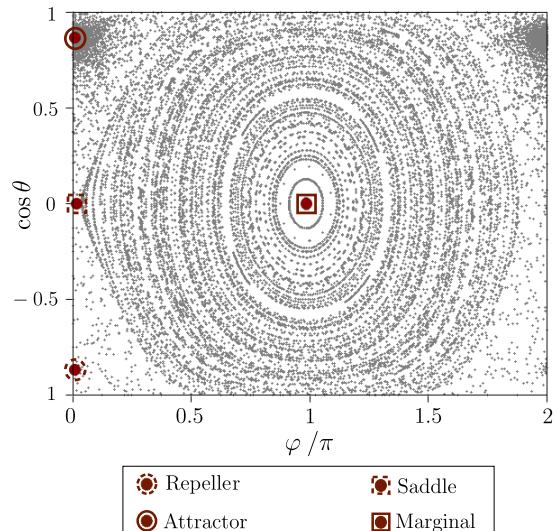


FIG. 2. Phase portrait of the dynamical system in Eq. (3) for  $p = 2$  and  $q = 1$ . The parameters  $\omega_x = \omega_z = 1$ ,  $\delta\Gamma = 0.2\omega_x$  are chosen to be in the coexistence region. The black lines are the trajectories associated to different initial conditions, while the red dots are the stationary states of the system, two ferromagnetic solutions and two paramagnetic ones. Of the two ferromagnetic solutions, the positive one (solid circle) is stable and attracts the trajectories, while the negative one (dashed circle) is unstable and therefore repels them. The negative paramagnetic solutions (solid square) generate periodic orbits associated to the BTC behavior, while the positive paramagnetic one (dashed square) separates the ferromagnetic basin of attraction from the BTC one.

In Fig. 2 we show the phase portrait for the phase coexistence region, with  $\omega_x = \omega_z$  and  $\delta\Gamma = 0.2\omega_z$  as a function of the polar angle  $\varphi$  and its conjugate variable  $\cos \theta$ , with  $\theta$  the azimuthal angle. The red dots are the solutions of the system in Eq. (3), with the left-hand side equal to zero, while the grey lines are trajectories associated with different initial conditions. Each fixed point clearly influences the trajectories in a different way: the ferromagnetic state with positive (solid circle) magnetization ( $\cos \theta > 0$ ) is stable and therefore attracts the nearby trajectories, while the negative (dashed circle) one repels them. The marginal paramagnetic (solid square) solution at  $(\varphi = \pi, \cos \theta = 0)$ , instead, generates the periodic orbits associated with the time crystal behavior. Finally, there is a second paramagnetic “saddle” (dashed square) fixed point at  $(\varphi = 0, \cos \theta = 0)$  which separates the region of influence of all other stationary solutions.

### C. $x$ -interactions ( $p = 1, q = 2$ )

Let us now switch the direction of the interaction and the transverse field in the Hamiltonian, i.e. we consider a fully connected Ising chain in transverse field with interactions along the  $\hat{x}$  direction, described by ( $p = 1, q = 2$ )

in Eq. (1)):

$$\hat{H}^{(x)} = -N \left( \omega_x \hat{J}_x^2 + \omega_z \hat{J}_z \right). \quad (9)$$

Although the closed systems described by Eqs. (5) and (9) are identical, the specific form of the Lindblad operators leads to very different dynamics when coupling to the environment. In this case, there is a single line in the phase diagram with time crystal order, corresponding to  $\omega_z = 0$ : as soon as  $\omega_z > 0$  BTCs are destroyed and the system relaxes toward a stable fixed point, that can be either x-paramagnetic ( $X = 0$ ), or x-ferromagnetic ( $|X| > 0$ ). In Fig. 3 we show the phase portrait for  $\omega_z = \omega_x = 1$  and  $\delta\Gamma = 0.2\omega_x$ . In order to avoid the singularities at the poles of the unit sphere, here we use a different parametrization with respect to standard polar coordinates

$$\mathbf{R} = (\cos \theta', \sin \theta' \cos \varphi', \sin \theta' \sin \varphi') \quad (10)$$

where  $\varphi'$  and  $\theta'$  are the polar and azimuthal angle defined with respect to the  $x$ -axis. Looking at the phase portrait in panel (a) of Fig. 3 we identify two attractive x-ferromagnetic states (solid circles), reflecting the  $\mathbb{Z}_2$  symmetry of the Hamiltonian, and one repelling x-paramagnetic state (dashed circle) with  $X = 0$  and  $Z = -1$ .

Although, at first sight, it might appear that this point is surrounded by closed orbits, actually the trajectories are escaping from the fixed point, describing a *spiral*. This is more evident by looking at the behavior on the Bloch sphere in panel (b) of Fig. 3 of the corresponding blue trajectory in the phase space. Thus, in contrast with the previous situation, there are no periodic orbits associated with a time-crystalline phase. This holds for any nonzero value of  $\omega_z$ : the stronger the transverse field, the faster the trajectories will collapse. Finally, the last x-paramagnetic solution (dashed square) separates the basin of attraction of the positive x-ferromagnetic solution to that of the negative x-ferromagnetic one.

#### IV. BTCS EXISTENCE CONDITION 1: SYMMETRY

In this section, we present the mean-field and exact finite- $N$  dynamics of the generalized  $p$ -spin model. From our results, it emerges that to observe BTCs the Hamiltonian needs to be  $\mathbb{Z}_2$  invariant and the Lindblad operators must break explicitly this symmetry. This implies that the BTC phase exists only for even values of  $p$ , while  $q$  can be either even or odd.

##### A. Mean-field analysis

Let us explore the mean-field dynamics of the generalized  $p$ -spin model in Eq. (1) to discuss the symmetry

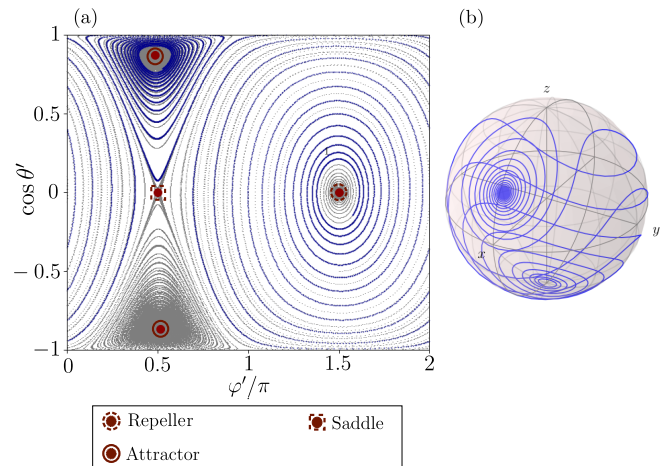


FIG. 3. Panel (a): Phase portrait of the dynamical system in Eq. (3) for  $p = 1$  and  $q = 2$ . The parameters  $\omega_z = \omega_x$ ,  $\delta\Gamma = 0.2\omega_x$  correspond to a ferromagnetic phase. The black lines are the trajectories associated to different initial conditions, while the red dots are the stationary states of the system, two x-ferromagnetic ( $|X| > 0$ ) solutions (solid circles) and two x-paramagnetic ( $X = 0$ ) ones. We notice that the x-ferromagnetic solutions are both stable, reflecting the  $\mathbb{Z}_2$  symmetry of the Hamiltonian. The negative x-paramagnetic solution (dashed circle) is a repeller, while the other one (dashed square) separates the positive x-ferromagnetic basin of attraction from the negative x-ferromagnetic one. The Bloch sphere in panel (b) shows a particular trajectory which well represent the behavior close to attractive and repulsive fixed points. The same trajectory is depicted with a continuous blue line also in the main panel.

conditions necessary to BTCs. The more intuitive way to do so is by looking at the phase portrait for different values of  $p$  and  $q$ . From now on we will parametrize the sphere as in Eq. (8). All the results (unless specified) are obtained with  $\omega_x = \omega_z$  and  $\delta\Gamma = 0.2\omega_z$ .

First, we fixed  $q = 1$ . In the top panels of Fig. 4 we show the phase portrait for  $p = 3$  (a) and  $p = 4$  (b), a non-symmetric and to a  $\mathbb{Z}_2$ -symmetric Hamiltonian, respectively. At first sight, the two figures seem to share the same physics: the trajectories are either attracted toward a positive ferromagnetic stationary state or stuck into periodic orbits. Actually, this is not true since the trajectories surrounding the paramagnetic solutions, as shown in the bottom panels, are very slowly damping toward a time-independent value.

In the bottom panels of Fig. 4 we plot the trajectories of the longitudinal magnetization, that in the phase portrait are highlighted in blue and red on the Bloch sphere. From these figures emerge that, while in the case  $p = 4$  (d) we have a closed orbit, for  $p = 3$  (c) the trajectories are attracted toward the ferromagnetic solution with damping (which can be very slow, depending on the initial conditions) that eventually suppresses the oscillations, ruling out the possibility of BTCs. An analysis of the oscillations amplitude  $A(t)$  shows, indeed, that for

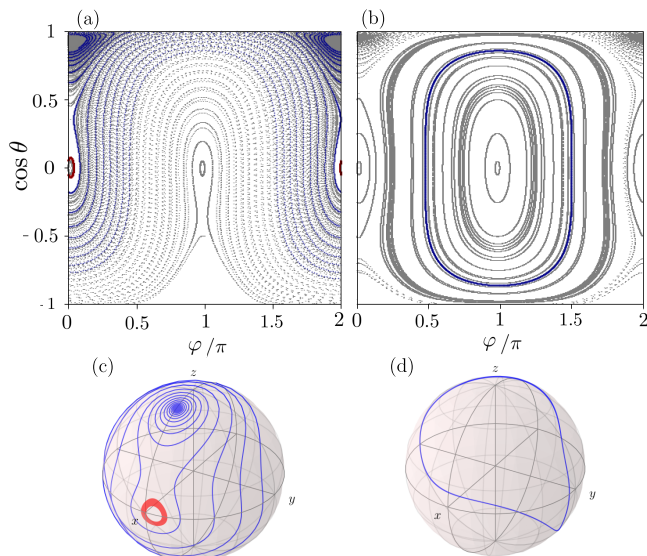


FIG. 4. Top panels: Phase portraits obtained by solving Eq. (3) with  $q = 1$ ,  $p = 3$  (a) and  $p = 4$  (b), fixed  $\omega_z = \omega_x$  and  $\delta\Gamma = 0.2\omega_z$ . The red trajectories correspond to the initial condition  $\varphi_0 = 0.10$  and  $\theta_0 = 1.47$ . Both diagrams present two ferromagnetic solutions and two paramagnetic ones. The ferromagnetic solutions are in both cases one attractive and the other repelling trajectories. The nature of the paramagnetic solutions, instead, depends on the value of  $p$ . In fact, only for  $p = 4$  (d), namely the  $\mathbb{Z}_2$ -symmetric case, we have a marginal fixed point generating periodic orbits, while for  $p = 3$  (c) it slowly attracts the trajectories. Bottom panels: typical trajectories depicted on the Bloch sphere for  $p = 3$  (c) and  $p = 4$  (d); the same trajectories are highlighted with the same color also in the phase portraits in (a) and (b). The “thickness” of the red trajectory in (c) signals that it is slowly spiralling towards the  $X = 1$  fixed point.

$p > 1$  it decreases in time with a  $p$ -dependent power law. When  $q = 1$  the scaling is

$$A(t) = B t^{-\frac{1}{p-1}}, \quad (11)$$

where the precise value of  $B$  depends on the other system parameters.

Let us now consider the case of a  $\mathbb{Z}_2$  preserving Hamiltonian by fixing  $p = 2$ . In the top panels of Fig. 5 we plot the phase portraits for  $q = 1, 2, 3, 4$ . Although the complexity of the phase portrait increases by increasing  $q$ , there are always some periodic orbits signaling the presence of BTCs. The blue and the orange diamonds in panel (a) Fig. 5 mark the parameters used in Fig. 7. The bottom panels show the trajectories in time of the longitudinal magnetization evaluated over the red trajectories, confirming the persistence of the oscillations and the emerging of a time-crystal order.

Although we do not have rigorous proof, our numerical analysis strongly suggests our claim on the symmetry requirement: if the dissipation does not break the discrete

symmetry of the Hamiltonian, closed periodic orbits do not appear.

## B. Finite- $N$ analysis

To corroborate the mean-field analysis done so far, we solve the exact quantum dynamics in finite systems and present three indicators that identify the BTC phase: (i) the oscillations of the expectation value of the magnetization and the link between the damping rate and the system size  $N$ , (ii) the part of the Liouvillian spectrum closest to the origin of the complex plane, (iii) the structure of the stationary state density matrix  $\hat{\rho}_0$ .

### 1. Oscillations of the magnetization

Since the Lindblad equation conserves the total spin, we can restrict the analysis to the sector of the Hilbert space with total spin  $S^2 = \frac{N}{2}(\frac{N}{2} + 1)$ . This allows us to access numerically systems of the order  $N \sim 10^2 - 10^3$ , depending on whether we are interested in the Liouvillian spectrum or only in the time evolution. All numerical results have been obtained using the QuTiP [90, 91] Python package. In what follows, we mainly focus our attention on the Hamiltonian in Eq. (5), corresponding to the choice  $p = 2$ ,  $q = 1$ .

First, let us consider the finite- $N$  dynamics in the BTC phase. Figure 6 shows the main features of a typical trajectory of the magnetization in the BTCs phase. Differently from the mean-field case, the magnetization presents oscillations decaying with a damping strength that decreases for increasing system size  $N$ , which finally vanishes in the thermodynamic limit. By performing a data collapse of the oscillation amplitudes, we found that the decay rate follows a power-law compatible with  $N^{-0.4}$  (data not shown). The only exception is the free spin case in Eq. (4), with  $\omega_z = 0$ , studied in detail in Ref. [40], where the decay rate decreases as  $N^{-1}$ .

The period of the oscillations, instead, is practically size-independent and, in fact, the Fourier spectrum is always peaked around the same frequency with a small broadening that reduces by increasing  $N$ . In the BTC phase, this behavior is independent of the initial condition and, qualitatively, it holds  $\forall p$  (even).

In the intermediate phase, periodic orbits and relaxation dynamics coexist in the thermodynamic limit. When one focuses on finite-size effects, this behavior persists for a finite time window, as shown in Fig. 7. Depending on the initial conditions, the trajectory might display both  $N$ -dependent damped oscillations or a size-independent relaxation toward the ferromagnetic stationary state. Eventually, this apparent bistability breaks after a time scale  $\tau_N \sim N$ , when the trajectory deviates from the time-crystal density matrix to slowly approach the unique steady state (inset of Fig. 7). The relative Liouvillian spectrum is qualitatively similar to that of the

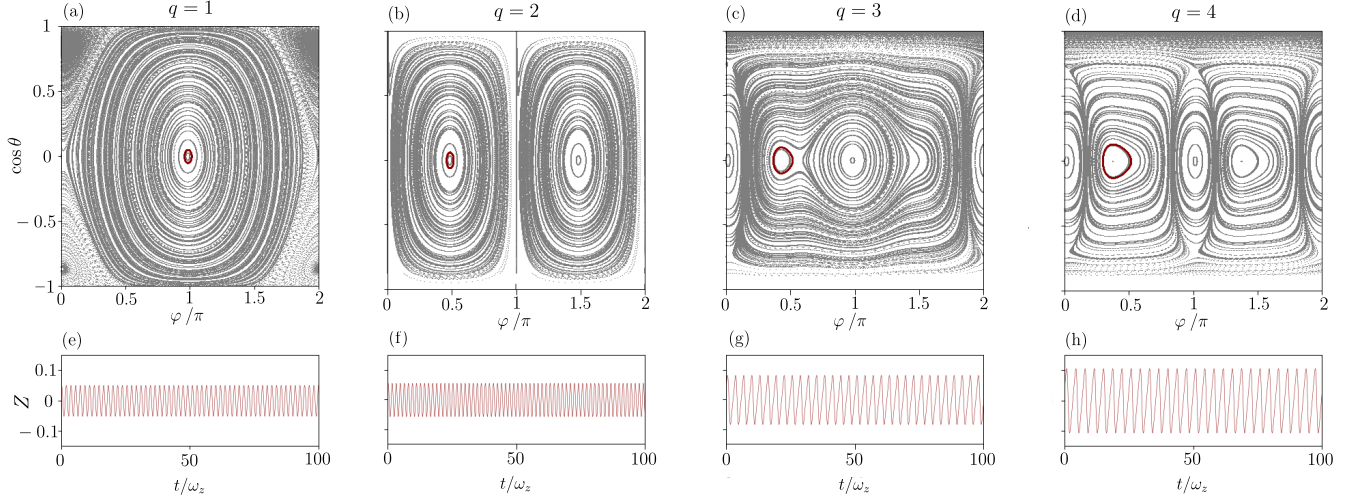


FIG. 5. Top panels: phase portraits for  $p = 2$  and  $q = 1$  (a),  $q = 2$  (b),  $q = 3$  (c),  $q = 4$  (d). We set  $\omega_x = \omega_z$ ,  $\delta\Gamma = 0.2\omega_z$ . For all the values of  $q$ , we observe periodic orbits, indicating BTCs. The blue and orange squares in panel (a) Fig. 5 mark the parameters used in Fig. 7. The bottom panels show the behavior in time of the longitudinal magnetization evaluated over the red trajectories in the relative phase portrait (corresponding to the initial conditions  $\varphi_0 = 3.10$ ,  $\theta_0 = 1.47$  for  $q = 1$  (e) and  $\varphi_0 = 1.57$ ,  $\theta_0 = 1.47$  for  $q = 2$  (f),  $q = 3$  (g),  $q = 4$  (h)). We observe that the oscillations persist in time independently on the value of  $q$  confirming that the BTC phase is not affected by the interactions along the  $\hat{\mathbf{x}}$  direction.

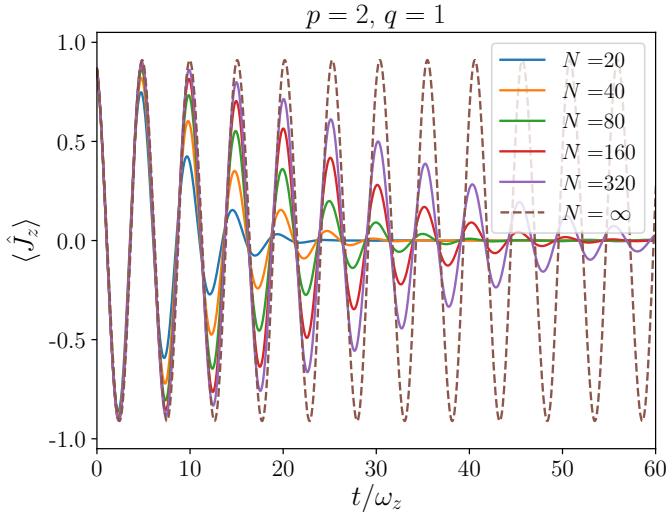


FIG. 6. Magnetization  $\langle \hat{J}_z \rangle$  versus time  $t$ , for several values of the system size  $N$  and interaction ranks  $p = 2$ ,  $q = 1$ . The dashed line corresponds to the trajectory in the thermodynamic limit, obtained through the mean-field equations (3). The other parameters of the model are  $\omega_x = 3\omega_z$  and  $\delta\Gamma = 0.2\omega_z$ .

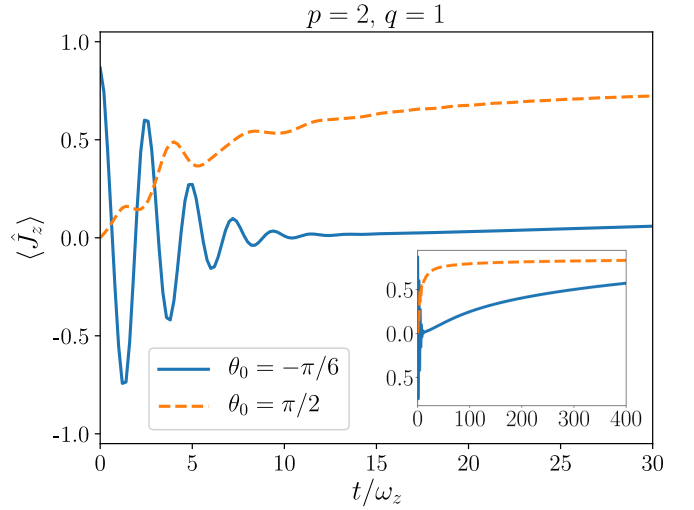


FIG. 7. Comparison of the time dependence of the average magnetization for two different initial conditions: all spins aligned along the direction  $(\theta_0, \phi_0) = (-\pi/6, 0)$  (solid blue curve) and  $(\theta_0, \phi_0) = (-\pi/2, 0)$  (dashed orange curve). The system size is  $N = 100$  and the other Hamiltonian parameters are  $p = 2$ ,  $q = 1$ ,  $\omega_x = \omega_z$ . The dissipation is  $\delta\Gamma = 0.1\omega_z$ . The inset shows the same data on a longer time scale, where one can see the slow relaxation of the trajectory corresponding to the boundary time crystal towards the ferromagnetic stationary state.

BTC phase with a stationary state that is ferromagnetic instead of paramagnetic.

## 2. Liouvillian spectrum

The properties depicted above are reflected in the eigenspectrum of the Liouvillian. In Fig. 8 we show the behavior of the real and the imaginary part (left and right panels, respectively) of the eigenvalues as a function of the system size  $N$  for the BTCs phase, in (a) and (c), and the ferromagnetic phase in (b) and (d).

In the BTC phase, see Fig. 8(a), the real part of the spectrum roughly divides into a set of real eigenvalues that decreases as  $\text{Re}[\lambda^{(N)}] \sim N^{-1}$ , and a set of complex eigenvalues associated with the BTCs (blue circles) with a much slower decay. Again, the only exception is the free spin case in which, as mentioned, we find a power-law behavior. Because of the computational effort needed to diagonalize the Liouvillian superoperator, it is hard to extract a precise scaling; however, we found that its behavior is compatible with the power-law decay  $N^{-0.4}$ , in agreement with the damped oscillations discussed above.

The imaginary part in Fig. 8(c), instead, clearly saturates to values independent from  $N$ . Surprisingly, the oscillation frequency of the magnetization is not linked to the values of the imaginary part, contrary to what happens in the free case. It is not yet clear the origin of this mismatch, but it might be due to interference between eigenstates of the Liouvillian with frequencies that are not commensurate.

In (b) and (d), we plot the Liouvillian eigenvalues for the ferromagnetic phase. In this case, the behavior of the real part of the eigenvalues is markedly different from the previous one. There is still at least one real eigenvalue decreasing as  $N^{-1}$ , suggesting the possibility of multiple steady-states in the thermodynamic limit. Despite this, the Liouvillian gap is much larger than the corresponding one in the BTC phase, as one can appreciate from the different scales of the two vertical axes. More importantly, the real part of the lowest complex eigenvalues (blue circles) do not display any dependence on  $N$ , which means that any oscillatory behavior is doomed to decay also in the thermodynamic limit.

## 3. Steady-state density matrix

Finally, we would like to briefly comment on the stationary state density matrix  $\hat{\rho}_0$ . When the system is in the BTC phase, the density matrix  $\hat{\rho}_0$  of the stationary state for finite size  $N$  is independent on the choice of individual parameters and acquires the characteristic structure shown in Fig. 9(a). Besides some corrections of the order  $O(N^{-2})$ ,  $\hat{\rho}_0$  is proportional to the identity matrix, where all eigenstates of  $\hat{S}_z$  are populated uniformly. This suggests that there is an emergent  $\mathbb{Z}_{N+1}$  symmetry, generated by a unitary ladder operator  $\hat{Q}$  that acts on the eigenstates  $|m\rangle$  of  $\hat{S}_z$  as  $\hat{Q}|m\rangle = |m+1\rangle$ .

At finite size  $N$  this symmetry is not exact, but it gets closer to an actual  $\mathbb{Z}_{N+1}$  invariance for increasing values

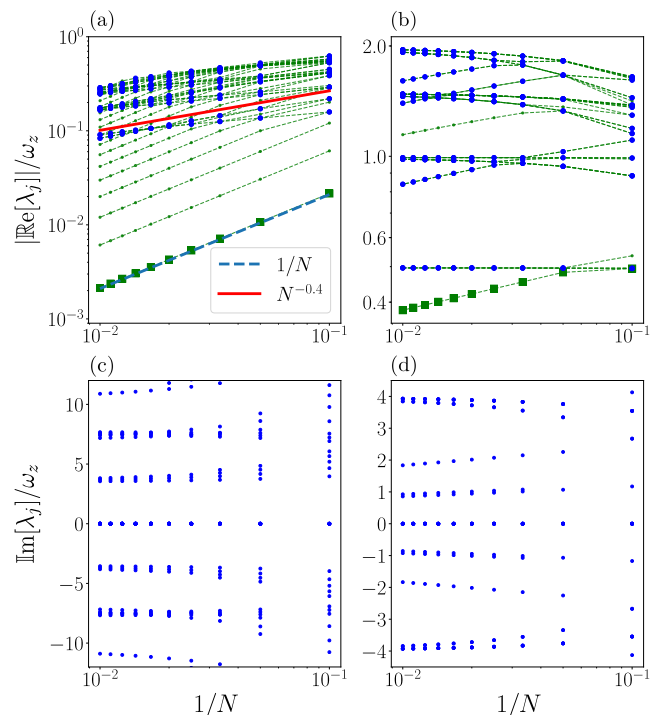


FIG. 8. Real and imaginary parts vs  $1/N$  of the 21 eigenvalues of the Liouvillian with  $\text{Re}[\lambda_i^{(N)}]$  closest to zero. The large blue circles in the upper panels highlight eigenvalues with a nonzero imaginary part. The dashed blue line in (a) and highlights the  $1/N$  scaling of the Liouvillian gap (green squares); the solid red line shows the possible  $N^{-0.4}$  scaling of the eigenvalues with nonzero imaginary parts. (a) and (c): BTC phase with  $p = 2$ ,  $q = 1$ ,  $\omega_x = 3\omega_z$ , and  $\delta\Gamma = 0.2\omega_z$ . (b) and (d): ferromagnetic phase with  $p = 2$ ,  $q = 1$ ,  $\omega_x = 0.25\omega_z$ , and  $\delta\Gamma = 0.5\omega_z$ .

of  $N$ , until it becomes a  $U(1)$  symmetry in the thermodynamic limit. A similar mechanism to simulate a  $U(1)$  lattice gauge theory has been proposed in Ref. [92]. In the present case, we argue that this  $U(1)$  symmetry is associated to the closed orbits arising in the mean-field description of the thermodynamic limit, where the dynamics keeps the memory of the initial state, modulo a rotation. This result is further validated by the correspondence between the emergence of time crystals and dissipative phase transitions as shown in Ref. [69].

As a consequence of its structure, the BTC steady-state density matrix *cannot* be described with a mean-field approximation, meaning that it cannot be written as a direct product of single spin density matrices, since the fluctuations of the magnetization components *diverge* in the thermodynamic limit. By a simple calculation, see App. C, it is possible to show that it does not exist a factorized density matrix  $\hat{\rho}_0$  giving  $\text{Tr}[\hat{\rho}_0\hat{S}_x] \simeq \text{Tr}[\hat{\rho}_0\hat{S}_y] \simeq \text{Tr}[\hat{\rho}_0\hat{S}_z] \simeq 0$ , while preserving  $\hat{S}^2$ . It is more appropriate to think of the finite size steady state as the average of the magnetization vector

over a BTC trajectory in the thermodynamic limit. This picture holds for any parameter choice where the BTC phase exists and it is in perfect agreement with the analysis of the semiclassical trajectories in Ref. [75].

In the ferromagnetic and mixed phases, the stationary-state density matrix resembles, instead, a coherent spin state, with a degree of spin squeezing [93] which depends on the values of the Hamiltonian parameters,  $p$  and  $\delta\Gamma$  in particular. As an example, in Fig. 9(b) we show the absolute value of  $\hat{\rho}_0$  for  $p = 3$ . It is evident that, differently from the BTC steady state, the steady state also displays appreciable coherences. This feature provides further interesting elements on the generality of the model of Eq. (1) also with regard to the steady-state properties of the driven-dissipative system, e.g., for subradiant and subradiance, coherence and spin squeezing [62, 94].

To compare quantitatively the two cases, in Fig. 9(c) we plot the purity of the density matrix  $\text{Tr}[\hat{\rho}_0^2]$  as a function of the system size  $N$ . In the BTC phase, corresponding to  $p$  even, the purity is practically the lowest possible  $(N + 1)^{-1}$ , the same as the identity matrix.  $\hat{\rho}_0$  is indeed a mixed state without coherences which satisfies  $\text{Tr}[\hat{\rho}_0 \hat{S}_x] \simeq \text{Tr}[\hat{\rho}_0 \hat{S}_y] \simeq \text{Tr}[\hat{\rho}_0 \hat{S}_z] \simeq 0$ . For odd values of  $p$  the purity is much higher, showing that the steady-state density matrix is quantitatively and qualitatively different in the two phases.

## V. BTCS EXISTENCE CONDITION 2: COLLECTIVE DISSIPATION

In this section, we show that only in the presence of collective dissipation processes only, the dynamics of Eq. (3) displays time crystallinity. To this purpose, we follow the dynamics of the simplest time crystal Hamiltonian described in Eq. (5), i.e. when  $p = 2$  and  $q = 1$ , coupled to a bath through a string of jump operators  $J_s^\pm = \sum_i^{N_s} \sigma_i^\pm / N_s$ , with  $N_s \leq N$ . Note that these Lindblad operators do not conserve the total angular momentum  $J^2$ . The mean-field equations of motion read

$$\begin{cases} \dot{X} = 2p\omega_z Z^{p-1} Y - 2 \left( \delta\Gamma Z_s + \frac{\bar{\Gamma}}{N_s} \right) X_s, \\ \dot{Y} = 2XZ (q\omega_x X^{q-2} - p\omega_z Z^{p-2}) - 2 \left( \delta\Gamma Z_s + \frac{\bar{\Gamma}}{N_s} \right) Y_s, \\ \dot{Z} = -2q\omega_x Y X^{q-1} + 2\delta\Gamma \left( 1 - Z^2 + \frac{1}{N_s} \right) - \frac{2\bar{\Gamma}}{N_s} Z_s, \end{cases} \quad (12)$$

where we have defined  $\bar{\Gamma} = \Gamma_\uparrow + \Gamma_\downarrow$  and  $\alpha_s = \langle J_\alpha^s \rangle$ . The results in Sec. III are recovered in the thermodynamic limit when  $N_s = N$ . In (a) of Fig. 10 we show the trajectories of the magnetization  $Z$  as a function of time for three different values of  $N_s = 10, 20, 50$ ; with  $\delta\Gamma = 0.2\omega_z$  and  $\omega_x = 1.1\omega_z$ . By comparing with the collective decay trajectory (gray dashed line) it emerges a twofold effect, both on the phase and on the amplitude of the oscillations, due to the finite range of the dissi-

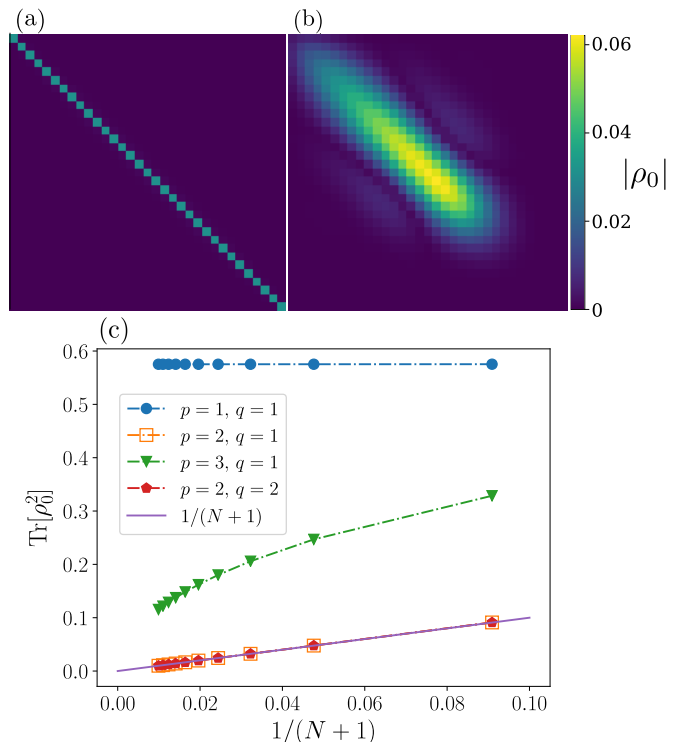


FIG. 9. (Absolute value of the stationary-state density matrix for  $N = 30$ ,  $q = 1$ ,  $\omega_x = 3\omega_z$  and  $\delta\Gamma = 0.2\omega_z$ . In (a)  $p = 2$ , while in (b)  $p = 3$ . The density matrix elements are computed in the basis of the  $z$ -magnetization  $\hat{S}_z = \frac{N}{2} \hat{J}_z$ . (c): purity of the stationary-state density matrix  $\text{Tr}[\hat{\rho}_0^2]$  versus  $1/(N + 1)$  for several values of  $p$  and  $q$ . When the BTC phase is present, the purity is the lowest possible in the subspace of the Hilbert space where the dynamics is constrained, namely  $(N + 1)^{-1}$ . When the system relaxes towards a state with finite  $z$ -magnetization, instead, the purity is much larger.

pation operators. The trajectories for different values of  $N_s$  have slightly different periods, leading to a progressive dephasing which, however, has no relevant effect on the time-order. The more relevant consequence of the finite range of the bath operators is the damping that reduces the amplitude of the oscillations, eventually recovering a time-translational invariant state.

To analyze the  $N_s$  dependence of the time scale over which time order is destroyed, in (b) of Fig. 10 we plot the amplitude of the oscillations of  $Z$  as a function of time, for different  $N_s$ . The dashed lines, obtained by fitting the data, behave as

$$f(t) = \exp(-\beta t / N_s), \quad (13)$$

with  $\beta = 0.11$ . This means that the oscillations are exponentially damped in time, with a rate which decreases as a power law of the length of the string of the dissipation operators. Hence, only in the limit of global dissipation processes,  $N_s \rightarrow N$ , the oscillations persist for arbitrarily long time. This result confirms the intuition by Riera-Campeny and collaborators [95] that global dissipation

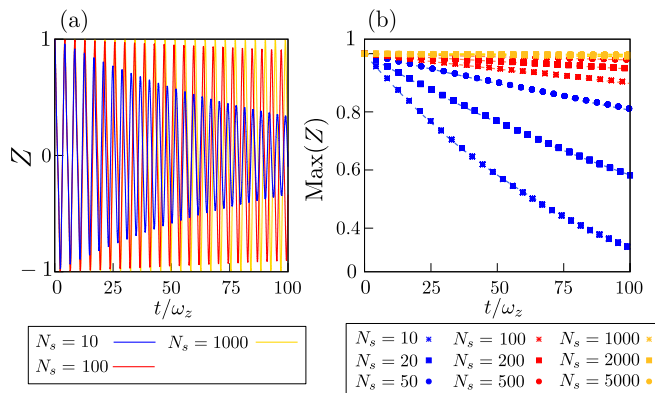


FIG. 10. (a): Trajectories of the longitudinal magnetization  $Z$  as a function of time for  $N_s = 10, 20, 50$ , fixed  $\delta\Gamma = 0.2\omega_z$  and  $\omega_x = 1.1\omega_z$ . The dashed line is the benchmark case with global dissipation processes  $N_s = N$ . Reducing the value of  $N_s$  the trajectories are affected by dephasing and damping effects that are as stronger as smaller  $N_s$ . (b): Oscillation amplitude of the  $Z$  component of the magnetization (full squares) as a function of time, for different values of  $N_s$ , and  $\delta\Gamma = 0.2\omega_z$  and  $\omega_x = 1.1\omega_z$ . The data are fitted with functions parametrized as  $f(t) = \exp(-\beta t/N_s)$  (dashed lines), with the fit parameter being  $\beta = 0.11$ .

processes are a key ingredient to observe the boundary time crystal. Our intuition is that this is an application of a more general condition that requires at least a conserved quantity in the dynamics. If so, in fact, the system cannot lose the information on the initial state during the evolution and is prevented to relax toward a time-independent state.

## VI. EXPERIMENTAL REALIZATIONS

In this section, we discuss how to experimentally implement the proposed model. We discuss two main aspects: relevant quantum simulation platforms and the engineering of higher-order spin interactions.

We have shown that the spin algebra can be implemented in ensembles of spin- $\frac{1}{2}$  with all-to-all connectivity. Rydberg atoms [96], trapped ions [97], artificial qubits in superconducting circuits [98], and color defects in diamond [99] are the most prominent platforms in which such all-to-all connectivity has been demonstrated. Let us point out that hybrid quantum systems [2, 100], such as color vacancies in diamond coupled to a single superconducting resonator offer the possibility to smooth out a long-range photon-mediated interaction on several emitters [99].

With regards to tuning the order of interactions,  $p$ , in the Hamiltonian of Eq. (1), the task can be divided in the standard cavity QED interactions,  $p, q \leq 2$  and in the more exotic many-body interactions,  $p, q > 2$ . In general, up to dipole approximation, the light-matter interaction that characterizes cavity QED systems involves

only two particles per time, i.e. annihilation/creation of bosonic/fermionic particles. The interaction mediated by bosons can in several cases be traced out, leading to effective spin-spin interactions ( $p = 2$ ). Spin-spin interactions are also the outcome of several microscopic processes, such as genuine magnetic interaction, internal-external degrees of freedom coupling in ions, Van der Waals forces in neutral atoms and so on. Using the quantum simulation paradigm [101], quantum phase transitions and dissipative phase transitions with long-range interactions have been engineered in trapped-ion and Rydberg-atom simulators [97, 102–104], although a power-law decay in the interaction length is common. In artificial atoms such as superconducting qubits, effective spin-spin interactions have been first proposed [105] and more recently implemented [98, 106], reproducing the physics of paradigmatic spin models, the Ising and Lipkin-Meshkov-Glick models.

The couplings for  $p, q > 2$  generally represent an indirect process and have been theoretically proposed in the context of spin glasses [107], which have become recently amenable to quantum simulation [108–110]. Direct interactions show up in the non-perturbative coupling between light and matter in the so-called ultrastrong and deep-strong coupling regimes [111], where it is not possible to arbitrarily tune higher-order coupling strengths, and where they occur in the boson-fermion framework.

Recently, the multiple excited states of natural and artificial atoms have been exploited to implement quantum systems beyond qubit systems, but with qudits or in general bosonic degrees of freedom, e.g., molecules or transmons in superconducting devices. It is important to point out that spin models can be mapped to bosons (and viceversa), e.g., with a Holstein-Primakoff approximation, but with the limitation of being in the diluted regime, i.e. where nonlinear effects are negligible [52].

With this regard, higher order interactions in bosonic systems based on superconducting circuit devices have recently been implemented, providing more freedom to tune higher-order interactions and suppress lower-order ones, exploiting nonlinearities in Josephson junctions [112–115], which can also be used to simulate spins with angular momentum greater than  $\frac{1}{2}$  [116, 117].

## VII. DISCUSSION AND CONCLUSION

In this work, we discussed two conditions for the existence of boundary time-crystals in a large class of generalized  $p$ -interaction spin models with dissipation, showing that the emergence of this non-equilibrium phase is strongly related to the symmetries and the conserved quantities of the Hamiltonian and how they are affected by the dissipation.

The first condition is that BTCs arise only if the spin Hamiltonian is  $\mathbb{Z}_2$ -symmetric and the Lindblad operators explicitly break this symmetry. If so, the mean-field trajectories of the magnetization display persistent oscil-

lations in time. This result resolves the apparent contradiction between Ref. [40] and Ref. [72]: in the latter the symmetry condition is not satisfied, hence the absence of BTCs.

This reflects an emerging U(1) symmetry of the equation of motion: closed orbits are invariant under rotations along the trajectory itself, meaning that the system preserves only partial information on the initial condition since all points on the same orbit lead to the same time-crystal dynamics. At finite-size  $N$ , instead, the oscillations are affected by a damping rate that decreases by increasing  $N$ . The U(1) symmetry of the thermodynamic limit now seems to appear as an *approximated* discrete  $\mathbb{Z}_{N+1}$  symmetry, similar to that argued in Ref. [92], as suggested by the characteristic profile of the stationary-state density matrix  $\hat{\rho}_0$  associated to the BTC phase. This condition provides a nice parallelism between boundary and discrete time crystals, a phase in which the subharmonic response is due to the exploration of different subsectors of some symmetric Hamiltonian or evolution operator [37–39, 43].

It is important to observe that the two conditions must be met in order to enter a BTC phase in the thermodynamic limit. A different, but similar phenomenology is that of decoherence-free subspaces [64–66], where time-dependent oscillations for long times are present at any system size, as investigated in the context of artificial giant atoms [64, 67, 70]. An example for the considered model is obtained for  $p = 0$ , hence  $\hat{H} \propto \hat{J}_x^q$  and a Lindblad jump operator equal to  $\hat{J}_x$  (which could be interpreted as a stochastic jump or global dephasing), or another jump operator commuting with the Hamiltonian, such as spin-squeezing dissipation,  $\hat{J}_x^2$ , or a collective dephasing channel.

These models preserve the  $\mathbb{Z}_2$  symmetry but are characterized by persistent oscillations at any system size  $N$ . Indeed, the Liouvillian spectrum at finite  $N$  is qualitatively independent from the coupling strength with the bath, indicating that collective dephasing does not induce different phases in our model and acts somehow “trivially” on the system.

The second condition regards the operators coupling the system with the bath: the time-crystal order is destroyed by dissipation processes that do not conserve the total angular momentum. In particular, we showed that if only a portion  $N_s < N$  of the system is coupled to the same external bath, the amplitude of oscillations decreases exponentially with  $N_s$ .

This result suggests that, more generally, BTCs arise only when there is at least one strong symmetry in the dynamics that prevents the system to lose information on the initial conditions and to attain a time-independent steady state. This draws an interesting parallelism with results that have shown how the symmetry sector to which an initial state belongs to can determine the current flows and quantum transport properties of the steady state [118]. However, we do not exclude that other kind of long range couplings between the system

and the environment may still allow for a stable BTC phase. This might be an interesting route to pursue to better understand if the robustness of the BTC phase is determined by the correlation length of the jump operators or strictly requires a homogeneous collective bath coupling.

Local dissipation induces also a dephasing in the mean-field trajectories, on top of the usual damping. This dephasing is probably due to the exploration of sectors with different total angular momentum; in the Dicke representation of permutational-invariant systems [52], this is equivalent to jumps between different Dicke ladders. Since different sectors have different Liouvillian spectra, the difference between the imaginary parts of the eigenvalues might indeed be responsible for the progressive dephasing of the oscillations. Understanding this mechanism could be an important step toward the full uptake of the BTC phenomenon. Moreover, it could give some hints on possible configurations in which the competition between global and local dissipation processes could give rise to interesting non-trivial phases of matters.

All the results of this work have been derived for a general class of dissipative spin models, which can be implemented in fully connected spin- $\frac{1}{2}$  ensembles, with a specific choice of the Lindblad dissipators, which can be engineered in quantum simulators, e.g., in superconducting-circuit-based quantum devices. However, the fact that BTCs are clearly associated with symmetry properties and not with the specific form of the Hamiltonian suggest that these criteria might apply for a wider class of systems and Lindblad operators. We anticipate that one of the most interesting directions for future investigations would be to explore the universality of our results, aiming for a general formulation of the existence conditions of BTCs in terms of symmetries and conserved quantities that may apply to a generic quantum many-body system.

Last, we would like to point out possible analogies between the mean-field limit in Eq. (3), for  $p = q = 1$ , and the Lorenz equations [119], which are one of the most known example of deterministic chaos in classical systems. This suggests the possible emergence of chaotic phases also in dissipative collective spin models, although the conservation of angular momentum  $X^2 + Y^2 + Z^2 = 1$ , due to the collective jump operators, might suppress chaos. However, time-dependent driving [120] or more complex Lindblad operators can probably be used to induce a transition from a regular to a chaotic phase. Hence, a deeper investigation of the connection between the semiclassical dynamics of open fully-connected quantum models and classical dynamical systems seems an interesting topic for future studies.

## ACKNOWLEDGMENTS

The authors acknowledge useful discussions with M. Burrello, M. Dalmonte, R. Fazio, F. Minganti, D. Rossini, G.E. Santoro, A. Silva and F.M. Surace. G.P. thanks

Giovanni Piccitto for useful comments. F.N. is supported in part by: NTT Research, Army Research Office (ARO) (Grant No. W911NF-18-1-0358), Japan Science and Technology Agency (JST) (via the CREST Grant No. JPMJCR1676), Japan Society for the Promotion of Science (JSPS) (via the KAKENHI Grant No. JP20H00134 and the JSPS-RFBR Grant No. JPJSBP120194828), the Asian Office of Aerospace Research and Development (AOARD) (via Grant No. FA2386-20-1-4069), and the Foundational Questions Institute Fund (FQXi) via Grant No. FQXi-IAF19-06. M.W. is supported by the Villum Foundation (Research Grant No. 25310). This project has received funding from the European Union's Horizon 2020 research and innovation program under the Marie Skłodowska-Curie grant agreement No. 847523 'INTER-ACTIONS'

### Appendix A: Derivation of the equations of motion

In this section we derive the mean-field equations of motion of Eq. (12). Let us assume to have a dynamics described by the master equation

$$\begin{aligned} \dot{\rho} &= -i[\hat{H}, \rho] + N\Gamma^\uparrow \left( J_s^+ \rho J_s^- - \frac{1}{2} \{J_s^- J_s^+, \rho\} \right) \\ &+ N\Gamma^\downarrow \left( J_s^- \rho J_s^+ - \frac{1}{2} \{J_s^+ J_s^-, \rho\} \right) \\ &= \dot{\rho}^c + \dot{\rho}^d. \end{aligned} \quad (\text{A1})$$

This evolution has two different contributions, a term that accounts for the coherent evolution,  $\dot{\rho}^c$ , and a term that accounts for the incoherent one,  $\dot{\rho}^d$ . The coherent part is simply obtained by evaluating the commutator with the Hamiltonian leading to

$$\begin{aligned} j_x^c &= 2 \sum_{n=0}^{p-1} J_z^{p-1-n} J_y J_z^n, \\ j_y^c &= -2 \sum_{n=0}^{p-1} J_z^{p-1-n} J_x J_z^n + 2gJ_z, \\ j_z^c &= -2gJ_y. \end{aligned} \quad (\text{A2})$$

We want to evaluate the incoherent contribution to the equations of motion for the expectation values of the spin operators. This is given by  $\langle J^\alpha \rangle = \text{Tr}(\dot{\rho}^d J^\alpha)$  leading to

$$\begin{aligned} \langle \dot{J}_\alpha \rangle &= -N\Gamma^\uparrow \text{Tr} \left( J_s^+ \rho J_s^- J_\alpha - \frac{1}{2} \{J_s^- J_s^+, \rho\} J_\alpha \right) \\ &+ N\Gamma^\downarrow \text{Tr} \left( J_s^- \rho J_s^+ J_\alpha - \frac{1}{2} \{J_s^+ J_s^-, \rho\} J_\alpha \right). \end{aligned} \quad (\text{A3})$$

By manipulating the equations we obtain

$$\begin{aligned} \langle \dot{J}_\alpha \rangle &= \frac{N i \delta \Gamma}{2} \langle \{J_s^x, [J_\alpha, J_s^y]\} - \{J_s^y, [J_\alpha, J_s^x]\} \rangle \\ &+ \frac{N \bar{\Gamma}}{2} \langle [J_s^x, [J_\alpha, J_s^x]] + [J_s^y, [J_\alpha, J_s^y]] \rangle \\ &= \frac{i \delta \Gamma}{2 N_s^2} \sum_{i,j} \sum_l^{N_s} \langle \{ \sigma_i^x, [\sigma_l^\alpha, \sigma_j^y] \} - \{ \sigma_i^y, [\sigma_l^\alpha, \sigma_j^x] \} \rangle \\ &+ \frac{\bar{\Gamma}}{2 N_s^2} \sum_{i,j} \sum_l^{N_s} \langle [\sigma_i^x, [\sigma_l^\alpha, \sigma_j^x]] + [\sigma_i^y, [\sigma_l^\alpha, \sigma_j^y]] \rangle \\ &= -\frac{\delta \Gamma}{2 N_s^2} \sum_{i,j} \langle \{ \sigma_i^x, \epsilon_{\alpha\gamma\beta} \sigma_j^\beta \} - \{ \sigma_i^y, \epsilon_{\alpha\gamma\beta} \sigma_j^\beta \} \rangle \\ &- \frac{\bar{\Gamma}}{2 N_s^2} \sum_{i,j} \langle [\sigma_i^x, \epsilon_{\alpha\gamma\beta} \sigma_j^\beta] + [\sigma_i^y, \epsilon_{\alpha\gamma\beta} \sigma_j^\beta] \rangle, \end{aligned} \quad (\text{A4})$$

where  $\delta\Gamma = \Gamma^\uparrow - \Gamma^\downarrow$  and  $\bar{\Gamma} = \Gamma^\uparrow + \Gamma^\downarrow$ .

### Appendix B: Derivation of the phase portrait

In this appendix we provide some details on the derivation of the phase portrait. In general, the spin operators in the semi-classical approximation can be parametrized on the Bloch sphere by giving the radius  $r$  of the sphere, the polar angle  $\varphi$  and the azimuthal one  $\theta$ . This mapping is singular in  $\theta = 0, \pi$ , therefore some care is needed in choosing the axis defining  $\varphi$  and  $\theta$ . The results of the paper have been derived by parametrizing the spin as

$$(X = r \sin \theta \cos \varphi, Y = r \sin \theta \sin \varphi, Z = r \cos \theta). \quad (\text{B1})$$

The only exceptions are the results in Subsec. III C, in which we assumed the polar angle to span the  $yz$  plane (namely, we fixed  $X = \cos \theta$ ). We will omit the derivation of this case since it can be obtained by simply extending the following calculations.

Eq. (B1) can be inverted leading to

$$\begin{aligned} r &= \sqrt{X^2 + Y^2 + Z^2}, \\ \varphi &= \arctan(Y/X), \\ \theta &= \arctan((X^2 + Y^2)/Z). \end{aligned} \quad (\text{B2})$$

By deriving and substituting the expressions of  $X, Y, Z$  in terms of  $r, \varphi, \theta$  we obtain, for the collective decay, the following equations of motion (since classically we have that  $\varphi$  and  $\cos \theta$  are conjugate variables, it is better to derive the equations for  $\cos(\theta)$  instead of  $\theta$ )

$$\begin{aligned} \dot{r} &= 2r\delta\Gamma \cos \theta (1 - r^2), \\ \dot{\varphi} &= -2\omega_z p \cos^{p-1} \theta + 2\omega_x q \cos \theta \sin^{q-2} \theta \cos^q \varphi, \\ \dot{\cos \theta} &= -(2\omega_x \sin^q \theta \cos^{q-1} \varphi \sin \varphi + 2\delta\Gamma (1 - \cos^2 \theta)) / r. \end{aligned} \quad (\text{B3})$$

We notice that  $r = 1$  is a fixed point, hence the dynamics is constrained on the surface of the Bloch sphere.

### Appendix C: Mean-field description of the totally symmetric subsector

Let us consider a generic single spin density matrix, parametrized as

$$\hat{\rho} = \begin{bmatrix} a & be^{-i\phi} \\ be^{i\phi} & 1-a \end{bmatrix} \quad (\text{C1})$$

where  $a$  and  $b$  are both real numbers. Its purity is defined as  $\mathcal{P} = \text{Tr}[\hat{\rho}^2] = \frac{1}{2} [(2a-1)^2 + 1 + 4b^2] \leq 1$ . The reason why we write it in this way will be clearer in the following.

We can construct a mean-field ansatz for the system by taking the tensor product of  $N$  identical spins described by density matrices as Eq. (C1)

$$\hat{\rho}_{\text{mf}} = \bigotimes_{j=1}^N \hat{\rho}_j. \quad (\text{C2})$$

We can compute the expectation value of the total spin  $\hat{S}^2 = \hat{S}_x^2 + \hat{S}_y^2 + \hat{S}_z^2$  on this state. First, let us rewrite it in terms of single-spin Pauli matrices

$$\hat{S}^2 = \frac{3}{4}N + \frac{1}{4} \sum_{k,j \neq k} \hat{\sigma}_j^x \hat{\sigma}_k^x + \hat{\sigma}_j^y \hat{\sigma}_k^y + \hat{\sigma}_j^z \hat{\sigma}_k^z. \quad (\text{C3})$$

Then, simple algebra leads to

$$\text{Tr}[\hat{\rho}_{\text{mf}} \hat{S}^2] = \frac{3}{4}N + \frac{1}{4}N(N-1) [(2a-1)^2 + 4b^2], \quad (\text{C4})$$

which can conveniently be rewritten in terms of the purity of the single-spin density matrix

$$\text{Tr}[\hat{\rho}_{\text{mf}} \hat{S}^2] = \frac{3}{4}N + \frac{1}{4}N(N-1)(2\mathcal{P}-1). \quad (\text{C5})$$

If  $\hat{S}^2$  is conserved and we consider in the maximally-polarized subsector, the total spin has to be equal to  $\frac{N}{2} (\frac{N}{2} + 1)$ , which is compatible with Eq. (C5) only if  $\mathcal{P} = 1$ . This means that a mean field ansatz for the density matrix *cannot* describe a mixed state in the maximally polarized subspace, but only pure ones. That is why to recover a mean-field approximation of mixed states such as that shown in Fig. 9, it is necessary to average over all magnetization vectors belonging to the same time-crystal trajectory.

- 
- [1] A. G. J. MacFarlane, J. P. Dowling, and G. J. Milburn, Quantum technology: the second quantum revolution, *Philos. T. R. Soc. A* **361**, 1655 (2003).
  - [2] Z.-L. Xiang, S. Ashhab, J. Q. You, and F. Nori, Hybrid quantum circuits: Superconducting circuits interacting with other quantum systems, *Rev. Mod. Phys.* **85**, 623 (2013).
  - [3] G. Kurizki, P. Bertet, Y. Kubo, K. Mølmer, D. Petrosyan, P. Rabl, and J. Schmiedmayer, Quantum technologies with hybrid systems, *Proc. Natl. Acad. Sci. USA* **112**, 3866 (2015).
  - [4] A. Acín, I. Bloch, H. Buhrman, T. Calarco, C. Eichler, J. Eisert, D. Esteve, N. Gisin, S. J. Glaser, F. Jelezko, S. Kuhr, M. Lewenstein, M. F. Riedel, P. O. Schmidt, R. Thew, A. Wallraff, I. Walmsley, and F. K. Wilhelm, The quantum technologies roadmap: a European community view, *New J. Phys.* **20**, 080201 (2018).
  - [5] M. Babadi, E. Demler, and M. Knap, Far-from-equilibrium field theory of many-body quantum spin systems: Prethermalization and relaxation of spin spiral states in three dimensions, *Phys. Rev. X* **5** (2015).
  - [6] M. Kollar, F. A. Wolf, and M. Eckstein, Generalized Gibbs ensemble prediction of prethermalization plateaus and their relation to nonthermal steady states in integrable systems, *Phys. Rev. B* **84** (2011).
  - [7] M. Stark and M. Kollar, Kinetic description of thermalization dynamics in weakly interacting quantum systems (2013), arXiv:1308.1610 [cond-mat.str-el].
  - [8] K. R. Fratus and M. Srednicki, Eigenstate thermalization and spontaneous symmetry breaking in the one-dimensional transverse-field Ising model with power-law interactions (2016), arXiv:1611.03992 [cond-mat.stat-mech].
  - [9] A. Safavi-Naini, M. L. Wall, O. L. Acevedo, A. M. Rey, and R. M. Nandkishore, Quantum dynamics of disordered spin chains with power-law interactions, *Phys. Rev. A* **99** (2019).
  - [10] A. Lerose, B. Žunkovič, A. Silva, and A. Gambassi, Quasilocalized excitations induced by long-range interactions in translationally invariant quantum spin chains, *Phys. Rev. B* **99** (2019).
  - [11] S. Pappalardi, A. Russomanno, B. Žunkovič, F. Iemini, A. Silva, and R. Fazio, Scrambling and entanglement spreading in long-range spin chains, *Phys. Rev. B* **98** (2018).
  - [12] T. Koffel, M. Lewenstein, and L. Tagliacozzo, Entanglement entropy for the long-range Ising chain in a transverse field, *Phys. Rev. Lett.* **109** (2012).
  - [13] Z.-X. Gong, M. Foss-Feig, F. G. Brandão, and A. V. Gorshkov, Entanglement area laws for long-range interacting systems, *Phys. Rev. Lett.* **119** (2017).
  - [14] G. Piccitto and A. Silva, Dynamical phase transition in the transverse field Ising chain characterized by the transverse magnetization spectral function, *Phys. Rev. B* **100** (2019).
  - [15] M. Kastner, N-scaling of timescales in long-range-N-body quantum systems, *J. Stat. Mech.* **2017**, 014003 (2017).
  - [16] P. Hauke and L. Tagliacozzo, Spread of correlations in long-range interacting quantum systems, *Phys. Rev. Lett.* **111**, 207202 (2013).
  - [17] L. Cevolani, G. Carleo, and L. Sanchez-Palencia, Protected quasilocality in quantum systems with long-range interactions, *Phys. Rev. A* **92**, 041603 (2015).

- [18] J. Lang, B. Frank, and J. C. Halimeh, Dynamical quantum phase transitions: A geometric picture, *Phys. Rev. Lett.* **121** (2018).
- [19] S. A. Weidinger, M. Heyl, A. Silva, and M. Knap, Dynamical quantum phase transitions in systems with continuous symmetry breaking, *Phys. Rev. B* **96** (2017).
- [20] M. Sandri, M. Schiró, and M. Fabrizio, Linear ramps of interaction in the fermionic Hubbard model, *Phys. Rev. B* **86** (2012).
- [21] V. Gurarie, Nonequilibrium dynamics of weakly and strongly paired superconductors, *Phys. Rev. Lett.* **103** (2009).
- [22] B. Sciolla and G. Biroli, Quantum quenches and off-equilibrium dynamical transition in the infinite-dimensional Bose-Hubbard model, *Phys. Rev. Lett.* **105** (2010).
- [23] G. Piccitto, B. Žunkovič, and A. Silva, Dynamical phase diagram of a quantum Ising chain with long-range interactions, *Phys. Rev. B* **100** (2019).
- [24] G. Piccitto and A. Silva, Crossover from fast to slow dynamics in a long range interacting Ising chain, *J. Stat. Mech.* **2019**, 094017 (2019).
- [25] T. Langen, R. Geiger, M. Kuhnert, B. Rauer, and J. Schmiedmayer, Local emergence of thermal correlations in an isolated quantum many-body system, *Nature Phys.* **9**, 640–643 (2013).
- [26] A. Rosch, D. Rasch, B. Binz, and M. Vojta, Metastable superfluidity of repulsive fermionic atoms in optical lattices, *Phys. Rev. Lett.* **101** (2008).
- [27] J. Berges, S. Borsanyi, and C. Wetterich, Prethermalization, *Phys. Rev. Lett.* **93**, 142002 (2004).
- [28] L. M. Sieberer, S. D. Huber, E. Altman, and S. Diehl, Dynamical critical phenomena in driven-dissipative systems, *Phys. Rev. Lett.* **110**, 195301 (2013).
- [29] L. M. Sieberer, M. Buchhold, and S. Diehl, Keldysh field theory for driven open quantum systems, *Rep. Prog. Phys.* **79**, 096001 (2016).
- [30] E. Altman, L. M. Sieberer, L. Chen, S. Diehl, and J. Toner, Two-dimensional superfluidity of exciton polaritons requires strong anisotropy, *Phys. Rev. X* **5**, 011017 (2015).
- [31] M. F. Maghrebi and A. V. Gorshkov, Nonequilibrium many-body steady states via Keldysh formalism, *Phys. Rev. B* **93**, 014307 (2016).
- [32] F. Wilczek, Quantum time crystals, *Physical Review Letters* **109** (2012).
- [33] V. Khemani, R. Moessner, and S. L. Sondhi, A brief history of time crystals (2019), [arXiv:1910.10745](https://arxiv.org/abs/1910.10745) [cond-mat.str-el].
- [34] K. Sacha and J. Zakrzewski, Time crystals: a review, *Rep. Prog. Phys.* **81**, 016401 (2017).
- [35] H. Watanabe and M. Oshikawa, Absence of quantum time crystals, *Phys. Rev. Lett.* **114** (2015).
- [36] V. K. Kozin and O. Kyriienko, Quantum time crystals from Hamiltonians with long-range interactions, *Phys. Rev. Lett.* **123**, 210602 (2019).
- [37] A. Russomanno, F. Iemini, M. Dalmonte, and R. Fazio, Floquet time crystal in the Lipkin-Meshkov-Glick model, *Phys. Rev. B* **95** (2017).
- [38] D. V. Else, B. Bauer, and C. Nayak, Floquet time crystals, *Phys. Rev. Lett.* **117** (2016).
- [39] F. M. Surace, A. Russomanno, M. Dalmonte, A. Silva, R. Fazio, and F. Iemini, Floquet time crystals in clock models, *Phys. Rev. B* **99**, 104303 (2019).
- [40] F. Iemini, A. Russomanno, J. Keeling, M. Schiró, M. Dalmonte, and R. Fazio, Boundary time crystals, *Phys. Rev. Lett.* **121**, 035301 (2018).
- [41] A. Riera-Campenya, M. Moreno-Cardoner, and A. Sanpera, Time crystallinity in open quantum systems, *Quantum* **4**, 270 (2020).
- [42] R. Hurtado-Gutiérrez, F. Carollo, C. Pérez-Espigares, and P. I. Hurtado, Building continuous time crystals from rare events, *Phys. Rev. Lett.* **125**, 160601 (2020).
- [43] A. Lazarides, S. Roy, F. Piazza, and R. Moessner, Time crystallinity in dissipative Floquet systems, *Phys. Rev. Research* **2** (2020).
- [44] B. Sciolla and G. Biroli, Quantum quenches, dynamical transitions, and off-equilibrium quantum criticality, *Phys. Rev. B* **88** (2013).
- [45] A. Leroze and S. Pappalardi, Origin of the slow growth of entanglement entropy in long-range interacting spin systems, *Phys. Rev. Research* **2** (2020).
- [46] A. Leroze and S. Pappalardi, Bridging entanglement dynamics and chaos in semiclassical systems (2020), [arXiv:2005.03670](https://arxiv.org/abs/2005.03670) [quant-ph].
- [47] T. E. Lee, S. Gopalakrishnan, and M. D. Lukin, Unconventional magnetism via optical pumping of interacting spin systems, *Phys. Rev. Lett.* **110**, 257204 (2013).
- [48] A. Biella, L. Mazza, I. Carusotto, D. Rossini, and R. Fazio, Photon transport in a dissipative chain of nonlinear cavities, *Phys. Rev. A* **91**, 053815 (2015).
- [49] A. Biella, F. Storme, J. Lebreuilly, D. Rossini, R. Fazio, I. Carusotto, and C. Ciuti, Phase diagram of incoherently driven strongly correlated photonic lattices, *Phys. Rev. A* **96**, 023839 (2017).
- [50] A. Biella, J. Jin, O. Viyuela, C. Ciuti, R. Fazio, and D. Rossini, Linked cluster expansions for open quantum systems on a lattice, *Phys. Rev. B* **97**, 035103 (2018).
- [51] F. Minganti, N. Bartolo, J. Lolli, W. Casteels, and C. Ciuti, Exact results for schrödinger cats in driven-dissipative systems and their feedback control, *Sci. Rep.* **6**, 26987 EP (2016).
- [52] N. Shammah, S. Ahmed, N. Lambert, S. De Liberato, and F. Nori, Open quantum systems with local and collective incoherent processes: Efficient numerical simulations using permutational invariance, *Phys. Rev. A* **98**, 063815 (2018).
- [53] D. Huybrechts and M. Wouters, Cluster methods for the description of a driven-dissipative spin model, *Phys. Rev. A* **99**, 043841 (2019).
- [54] D. Huybrechts, F. Minganti, F. Nori, M. Wouters, and N. Shammah, Validity of mean-field theory in a dissipative critical system: Liouvillian gap,  $\mathcal{PT}$ -symmetric anti-gap, and permutational symmetry in the XYZ model, *Phys. Rev. B* **101**, 214302 (2020).
- [55] M. M. Wouters, G. B. Mbeng, and G. E. Santoro, Polynomial scaling of the quantum approximate optimization algorithm for ground-state preparation of the fully connected  $p$ -spin ferromagnet in a transverse field, *Phys. Rev. A* **102**, 062404 (2020).
- [56] T. Brandes, Coherent and collective quantum optical effects in mesoscopic systems, *Phys. Rep.* **408**, 315–474 (2005).
- [57] D. Dylewsky, J. K. Freericks, M. L. Wall, A. M. Rey, and M. Foss-Feig, Nonperturbative calculation of phonon effects on spin squeezing, *Phys. Rev. A* **93** (2016).
- [58] R. Matsunaga, N. Tsuji, H. Fujita, A. Sugioka, K. Makise, Y. Uzawa, H. Tera, Z. Wang, H. Aoki, and

- R. Shimano, Light-induced collective pseudospin precession resonating with Higgs mode in a superconductor, *Science* **345** (2014).
- [59] V. Bapst and G. Semerjian, On quantum mean-field models and their quantum annealing, *J. Stat. Mech.* **2012**, P06007 (2012).
- [60] D. Vodola, L. Lepori, E. Ercolessi, and G. Pupillo, Long-range Ising and Kitaev models: phases, correlations and edge modes, *New J. Phys.* **18**, 015001 (2015).
- [61] F. Carollo and I. Lesanovsky, Proof of a nonequilibrium pattern-recognition phase transition in open quantum multimode Dicke models (2020), [arXiv:2009.13932](https://arxiv.org/abs/2009.13932) [[cond-mat.stat-mech](https://arxiv.org/abs/2009.13932)].
- [62] C. Sánchez Muñoz, B. Buča, J. Tindall, A. González-Tudela, D. Jaksch, and D. Porras, Symmetries and conservation laws in quantum trajectories: Dissipative freezing, *Phys. Rev. A* **100**, 042113 (2019).
- [63] J. Tindall, C. Sánchez Muñoz, B. Buča, and D. Jaksch, Quantum synchronisation enabled by dynamical symmetries and dissipation, *New J. Phys.* **22**, 013026 (2020).
- [64] B. Baumgartner and H. Narnhofer, Analysis of quantum semigroups with GKS-lindblad generators: II. general, *J. Phys. A* **41**, 395303 (2008).
- [65] B. Buča and T. Prosen, A note on symmetry reductions of the Lindblad equation: transport in constrained open spin chains, *New J. Phys.* **14**, 073007 (2012).
- [66] V. V. Albert and L. Jiang, Symmetries and conserved quantities in lindblad master equations, *Phys. Rev. A* **89**, 022118 (2014).
- [67] A. F. Kockum, G. Johansson, and F. Nori, Decoherence-free interaction between giant atoms in waveguide quantum electrodynamics, *Phys. Rev. Lett.* **120** (2018).
- [68] D. Manzano and P. Hurtado, Harnessing symmetry to control quantum transport, *Advances in Physics* **67**, 1 (2018).
- [69] F. Minganti, I. I. Arkhipov, A. Miranowicz, and F. Nori, Correspondence between dissipative phase transitions of light and time crystals (2020), [arXiv:2008.08075](https://arxiv.org/abs/2008.08075) [[quant-ph](https://arxiv.org/abs/2008.08075)].
- [70] B. Buča, J. Tindall, and D. Jaksch, Non-stationary coherent quantum many-body dynamics through dissipation, *Nat. Commun.* **10**, 1730 (2019).
- [71] Throughout the paper, the word “collective” identifies an operator which is the sum over all sites of single spin objects,  $\hat{O} = \sum_{j=1}^N \hat{o}_j$ . Notice that  $\hat{O}$  is invariant under permutation of the spin indices.
- [72] P. Wang and R. Fazio, Dissipative phase transitions in the fully-connected Ising model with  $p$ -spin interaction (2020), [arXiv:2008.10045](https://arxiv.org/abs/2008.10045) [[cond-mat.quant-gas](https://arxiv.org/abs/2008.10045)].
- [73] D. Manzano, A short introduction to the lindblad master equation, *AIP Advances* **10**, 025106 (2020).
- [74] M. Am-Shallem, A. Levy, I. Schaefer, and R. Kosloff, Three approaches for representing lindblad dynamics by a matrix-vector notation (2015), [arXiv:1510.08634](https://arxiv.org/abs/1510.08634) [[quant-ph](https://arxiv.org/abs/1510.08634)].
- [75] K. Seibold, R. Rota, and V. Savona, Dissipative time crystal in an asymmetric nonlinear photonic dimer, *Phys. Rev. A* **101** (2020).
- [76] E. Gardner, Spin glasses with  $p$ -spin interactions, *Nucl. Phys. B* **257**, 747 (1985).
- [77] M. Filippone, S. Dusuel, and J. Vidal, Quantum phase transitions in fully connected spin models: An entanglement perspective, *Phys. Rev. A* **83**, 022327 (2011).
- [78] V. Bapst and G. Semerjian, On quantum mean-field models and their quantum annealing, *J. Stat. Mech.* **2012**, P06007 (2012).
- [79] M. M. Wauters, R. Fazio, H. Nishimori, and G. E. Santoro, Direct comparison of quantum and simulated annealing on a fully connected Ising ferromagnet, *Phys. Rev. A* **96**, 022326 (2017).
- [80] B.-G. Englert and G. Morigi, Five lectures on dissipative master equations, *Lecture Notes in Physics*, 55–106 (2002).
- [81] The presence of purely imaginary Lyapunov exponents is necessary for the existence of the BTCs but it is not sufficient. For instance, it is possible to have purely imaginary Lyapunov exponents associated to slow spiraling trajectories in which the damping of the oscillations is a non-linear effect of the dynamics.
- [82] Notice that in the BTC phase every initial condition is associated to a different periodic orbit that keeps memory of the evolution of the initial state. This a substantial difference with the dynamics in presence of limit cycles in which all the trajectories eventually reach the same periodic orbit independently on the initial conditions.
- [83] A. Patra, B. L. Altshuler, and E. A. Yuzbashyan, Driven-dissipative dynamics of atomic ensembles in a resonant cavity: Quasiperiodic route to chaos and chaotic synchronization, *Ann. Phys.* **417**, 168106 (2020).
- [84] M. Gegg and M. Richter, Efficient and exact numerical approach for many multi-level systems in open system cqed, *New J. Phys.* **18**, 043037 (2016).
- [85] A. J. Daley, Quantum trajectories and open many-body quantum systems, *Adv. Phys.* **63**, 77–149 (2014).
- [86] S. Morrison and A. S. Parkins, Dissipation-driven quantum phase transitions in collective spin systems, *J. Phys. B* **41**, 195502 (2008).
- [87] T. E. Lee, C.-K. Chan, and S. F. Yelin, Dissipative phase transitions: Independent versus collective decay and spin squeezing, *Phys. Rev. A* **90** (2014).
- [88] A. Russomanno, F. Iemini, M. Dalmonte, and R. Fazio, Floquet time crystal in the Lipkin-Meshkov-Glick model, *Phys. Rev. B* **95**, 214307 (2017).
- [89] F. Dimer, B. Estienne, A. S. Parkins, and H. J. Carmichael, Proposed realization of the Dicke-model quantum phase transition in an optical cavity QED system, *Phys. Rev. A* **75**, 013804 (2007).
- [90] J. Johansson, P. Nation, and F. Nori, QuTiP: An open-source python framework for the dynamics of open quantum systems, *Comput. Phys. Commun.* **183**, 1760 (2012).
- [91] J. Johansson, P. Nation, and F. Nori, QuTiP 2: A python framework for the dynamics of open quantum systems, *Comput. Phys. Commun.* **184**, 1234 (2013).
- [92] E. Zohar, J. I. Cirac, and B. Reznik, Quantum simulations of gauge theories with ultracold atoms: Local gauge invariance from angular-momentum conservation, *Phys. Rev. A* **88**, 023617 (2013).
- [93] J. Ma, X. Wang, C. Sun, and F. Nori, Quantum spin squeezing, *Phys. Rep.* **509**, 89–165 (2011).
- [94] E. G. Dalla Torre, Y. Shchadilova, E. Y. Wilner, M. D. Lukin, and E. Demler, Dicke phase transition without total spin conservation, *Phys. Rev. A* **94**, 061802 (2016).
- [95] A. Riera-Campeny, M. Moreno-Cardoner, and A. Sanpera, Time crystallinity in open quantum systems,

- Quantum* **4**, 270 (2020).
- [96] L. Henriot, L. Beguin, A. Signoles, T. Lahaye, A. Browaeys, G.-O. Raymond, and C. Jurczak, Quantum computing with neutral atoms, *Quantum* **4**, 327 (2020).
- [97] J. Zhang, G. Pagano, P. Hess, A. Kyprianidis, P. Becker, H. Kaplan, A. Gorshkov, Z. Gong, and C. Monroe, Observation of a many-body dynamical phase transition with a 53-qubit quantum simulator., *Nature* **551**, 601 (2017).
- [98] S. Puri, C. K. Andersen, A. L. Grimsmo, and A. Blais, Quantum annealing with all-to-all connected nonlinear oscillators, *Nat. commun.* **8**, 1 (2017).
- [99] A. Angerer, K. Streltsov, T. Astner, S. Putz, H. Sumiya, S. Onoda, J. Isoya, W. J. Munro, K. Nemoto, J. Schmiedmayer, *et al.*, Superradiant emission from colour centres in diamond, *Nat. Phys.* **14**, 1168 (2018).
- [100] A. Clerk, K. Lehnert, P. Bertet, J. Petta, and Y. Nakamura, Hybrid quantum systems with circuit quantum electrodynamics, *Nat. Phys.* , 1 (2020).
- [101] I. Georgescu, S. Ashhab, and F. Nori, Quantum simulation, *Rev. Mod. Phys.* **86**, 153–185 (2014).
- [102] A. Keesling, A. Omran, H. Levine, H. Bernien, H. Pichler, S. Choi, R. Samajdar, S. Schwartz, P. Silvi, S. Sachdev, *et al.*, Quantum Kibble–Zurek mechanism and critical dynamics on a programmable Rydberg simulator, *Nature* **568**, 207 (2019).
- [103] P. Scholl, M. Schuler, H. J. Williams, A. A. Eberharter, D. Barredo, K.-N. Schymik, V. Lienhard, L.-P. Henry, T. C. Lang, T. Lahaye, A. M. Läuchli, and A. Browaeys, Programmable quantum simulation of 2d antiferromagnets with hundreds of rydberg atoms (2020), [arXiv:2012.12268](https://arxiv.org/abs/2012.12268) [quant-ph].
- [104] S. Ebadi, T. T. Wang, H. Levine, A. Keesling, G. Semeghini, A. Omran, D. Bluvstein, R. Samajdar, H. Pichler, W. W. Ho, S. Choi, S. Sachdev, M. Greiner, V. Vuletic, and M. D. Lukin, Quantum phases of matter on a 256-atom programmable quantum simulator (2020), [arXiv:2012.12281](https://arxiv.org/abs/2012.12281) [quant-ph].
- [105] D. I. Tsomokos, S. Ashhab, and F. Nori, Fully connected network of superconducting qubits in a cavity, *New J. Phys.* **10**, 113020 (2008).
- [106] K. Xu, Z.-H. Sun, W. Liu, Y.-R. Zhang, H. Li, H. Dong, W. Ren, P. Zhang, F. Nori, D. Zheng, and *et al.*, Probing dynamical phase transitions with a superconducting quantum simulator, *Science Advances* **6**, eaba4935 (2020).
- [107] T. R. Kirkpatrick and D. Thirumalai, p-spin-interaction spin-glass models: Connections with the structural glass problem, *Phys. Rev. B* **36**, 5388 (1987).
- [108] N. Roy, A. Sharma, and R. Mukherjee, Quantum simulation of long-range  $xy$  quantum spin glass with strong area-law violation using trapped ions, *Phys. Rev. A* **99**, 052342 (2019).
- [109] R. Harris, Y. Sato, A. Berkley, M. Reis, F. Altomare, M. Amin, K. Boothby, P. Bunyk, C. Deng, C. Enderud, *et al.*, Phase transitions in a programmable quantum spin glass simulator, *Science* **361**, 162 (2018).
- [110] P. Rotondo, M. Cosentino Lagomarsino, and G. Viola, Dicke simulators with emergent collective quantum computational abilities, *Physical Review Letters* **114**, 10.1103/physrevlett.114.143601 (2015).
- [111] A. Frisk Kockum, A. Miranowicz, S. De Liberato, S. Savasta, and F. Nori, Ultrastrong coupling between light and matter, *Nat. Rev. Phys.* **1**, 19–40 (2019).
- [112] A. F. Kockum and F. Nori, Quantum bits with josephson junctions, in *Fundamentals and Frontiers of the Josephson Effect* (Springer, 2019) pp. 703–741.
- [113] S. Touzard, A. Grimm, Z. Leghtas, S. O. Mundhada, P. Reinhold, C. Axline, M. Reagor, K. Chou, J. Blumoff, K. M. Sliwa, S. Shankar, L. Frunzio, R. J. Schoelkopf, M. Mirrahimi, and M. H. Devoret, Coherent oscillations inside a quantum manifold stabilized by dissipation, *Phys. Rev. X* **8**, 021005 (2018).
- [114] R. Lescanne, M. Villiers, T. Peronin, A. Sarlette, M. Delbecq, B. Huard, T. Kontos, M. Mirrahimi, and Z. Leghtas, Exponential suppression of bit-flips in a qubit encoded in an oscillator, *Nat. Phys.* **16**, 509–513 (2020).
- [115] A. Vrajitoarea, Z. Huang, P. Groszkowski, J. Koch, and A. A. Houck, Quantum control of an oscillator using a stimulated josephson nonlinearity, *Nat. Phys.* **16**, 211 (2020).
- [116] M. Neeley, M. Ansmann, R. C. Bialczak, M. Hofheinz, E. Lucero, A. D. O’Connell, D. Sank, H. Wang, J. Wenner, A. N. Cleland, *et al.*, Emulation of a quantum spin with a superconducting phase qudit, *Science* **325**, 722 (2009).
- [117] F. Nori, Quantum football, *Science* **325**, 689 (2009).
- [118] D. Manzano and P. I. Hurtado, Symmetry and the thermodynamics of currents in open quantum systems, *Phys. Rev. B* **90**, 125138 (2014).
- [119] E. N. Lorenz, Deterministic nonperiodic flow, *J. Atmos. Sci.* **20**, 130 (01 Mar. 1963).
- [120] A. Russomanno, R. Fazio, and G. E. Santoro, Thermalization in a periodically driven fully connected quantum Ising ferromagnet, *EPL* **110**, 37005 (2015).